The Closed-Loop Sideband Harmonic Suppression for CHB Inverter With Unbalanced Operation

Jiao, Ning; Wang, Shunliang; Ma, Junpeng; Cheng, Xiang ; Liu, Tianqi; Zhou, Dao; Yang, Yongheng

Closed-Loop Sideband Harmonic Suppression for CHB Inverter with Unbalanced Operation

Ning Jiao, *Student Member, IEEE*, Shunliang Wang, *Member*, *IEEE*, Junpeng Ma, *Member, IEEE*, Xiang Chen*,*
Tianqi Liu, *Senior Member*, *IEEE,* Dao Zhou*, Senior Member*, *IEEE*

Abstract- **For *N*-cells cascaded H-bridge (CHB) inverters based on unipolar double frequency phase-shifted pulse-width modulation (PS-PWM), the harmonic spectrum of the output voltage is degraded and difficult to be suppressed with unbalanced conditions (different dc voltages and/or modulation indices). This article proposes a closed-loop harmonic suppression scheme based on the PS-PWM technique, and the scheme is implemented with the "dq frame" to adjust cleverly the displacement angles of the triangular carriers online. The proposed method can effectively restrain harmonic magnitudes without the limitation of cells number and does not require complicated trigonometric function calculations. This method is not only applicable for all the operational conditions, but also suitable for harmonic optimization of different demands. Moreover, the principle of the symmetrical sideband harmonic suppression is also revealed. The effectiveness of the proposed method is verified by a down-scale test platform of the single-phase CHB inverter.[1]**

Index Terms—**harmonic suppression, cascaded H-bridge inverter, phase-shifted PWM.**

I. INTRODUCTION

The cascaded H-bridge (CHB) inverter is an attractive multilevel topology due to its advantages of high flexibility and extendibility [1]-[4]. The phase-shifted pulse-width modulation (PS-PWM) technique is the mature and traditional modulation method used in CHB inverters [5]-[6]. Yet, the superior quality of output voltage with the PS-PWM technique can be achieved [7] only in the ideal condition with equal dc voltages and modulation indices for different cells. Among possible applications, the CHB inverter has been used in the STATCOM [8]-[9] and solar photovoltaic [10]-[11], and it is a potential candidate for the integration of independent dc sources with different nature, such as PV-battery-hybrid system [12], batteries energy storage [13]. For these cases, different power management in each cell will present various behaviors in the cell dc voltages and cell modulation indices among cells. Taking these factors into account, sideband harmonics would be more dispersed and difficult to be suppressed in actual systems with non-ideal balanced conditions [7], [14].

To mitigate harmonics under unbalanced conditions, modified methods for PS-PWM have been widely studied in recent literature. For instance, the modified PS-PWM with proper shifting angles calculation for CHB inverters, only considering unbalanced dc voltages, has been proposed in [15], but it does not consider the variation in the modulation indices. This method is also extended to reduce the weighted total harmonic distortion (WTHD) of the cascaded multilevel STATCOM [16]-[17]. Yet, the differences of modulating

indices applied in all H-bridge submodules are ignored. In [18]-[20], the offline variable PS-PWM is further investigated addressing the possibility to operate the CHB inverter with mismatched modulation indices and different dc voltages. The variable PS-PWM technique is improved by introducing the sampling-time harmonic control in [21]-[22]. However, these techniques depending on inverse trigonometric functions are complicated, and the computational complexity grows and even has no analytical solution as the number of cells grows. Although some mathematical searching methods are introduced to solve this problem, such as Newton iteration method [23]-[25], recursive searching algorithm [26], particle swarm optimization [27]-[29], these methods are extremely complicated and some methods are difficult to be understood.

The existing modified PS-PWM technique mentioned above depends on the complicated solution of inverse trigonometric functions and offline mathematical searching methods. It becomes more complicated for CHB inverters with a large number of cells to achieve harmonic suppression. These methods are limited to the considered operational points and suitable conditions, due to the limitation of available controller memory and numerical solution limitation of inverse trigonometric functions. Therefore, these methods have great limitations in practical applications.

This article proposes a closed-loop harmonic suppression scheme to deal with the harmonic distortion for CHB inverters with unbalanced cells operation. The main contributions include: 1) the displacement angles of the triangular carriers in different cells can be regulated by online closed-loop control schemes, and harmonics can be suppressed by the proposed scheme in real-time. 2) the proposed method for CHB inverters can effectively operate in any number of cells. 3) the proposed method is not only applicable for any operating condition, but also suitable for different harmonic optimization demands. 4) The symmetrical sideband harmonics also have a good suppression performance based on the proposed harmonic suppression scheme.

The contents of this article are arranged as follows. In Section II, the system configuration and harmonic characteristics are introduced. In Section III, the offline variable-angle PS-PWM method (off. var. PS-PWM) is briefly described. In Section IV, the closed-loop harmonic suppression scheme and implement method are elaborated. In Sections V, simulation and experimental results are presented to validate the performance of the proposed method. Section VI concludes this article.

II. OVERVIEW OF CHB INVERTERS

In this section, the structure and operation principle of the CHB inverter is briefly described. Moreover, the harmonic generation principle is elaborated.

A. System Description

The schematic of the single-phase CHB inverter is shown in Fig. 1. The well-known phase-shifted pulse-width modulation (PS-PWM) technique is applied to generate the drive pulse [5]-[6]. i and N denote the cell number and the total number of cells ($i=1, 2, …, N$). u_{abi} and u_{ab} are the output voltage of the cell i, and the sum of all individual cell outputs, respectively. U_{dci} is the dc voltage in cell i. $T_{i1} \sim T_{i4}$ and $D_{i1} \sim D_{i4}$ represent the switching devices and diodes in cell i.
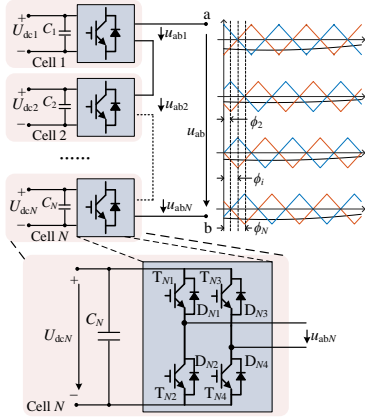

Fig. 1 Schematic of the single-phase CHB multilevel inverter.

Since all cells are connected in series, the output voltage of the CHB inverter, u_{ab}, can be described:

$$u_{ab} = \sum_{i=1}^{N} u_{abi} \tag{1}$$

For the conventional PS-PWM technique, the unipolar double frequency modulation with the carrier frequency f_c is applied in each cell. The phase displacement (ϕ_i in Fig. 1) of the i-th cell with respect to the phase angle of the first cell is defined:

$$\phi_i = (i-1)\frac{\pi}{N} \tag{2}$$

B. Harmonic Analysis

The voltage u_{abi} of cell i, generated by the PWM strategy [30], and its harmonic generation principle is described in Fig. 2. u_{ri}, u_{ci} represent the modulation signal and the triangle carrier signal in the i-th H-bridge. The harmonic spectrum of the voltage u_{abi} can be expressed as a summation of harmonic components and the fundamental component by the classical double Fourier series method [30]:

$$u_{abi} = M_i U_{dci} \cos(\omega_0 t + \theta_0)$$
$$+ \frac{2U_{dci}}{m\pi} J_{2n-1}(m\pi M_i)\cos[(m+n-1)\pi] \tag{3}$$
$$\times \cos\{[2m\omega_c + (2n-1)\omega_0]t + 2m\phi_i + (2n-1)\theta_0\}$$

where, M_i, ω_0, and θ_0 represent the modulation index, angular frequency, and initial phase angle of the modulation signal in cell i. ω_c is the angular frequency of the carrier signal. m and n are indices to account for carrier and baseband. J_{2n-1} is the Bessel function of order $2n-1$.
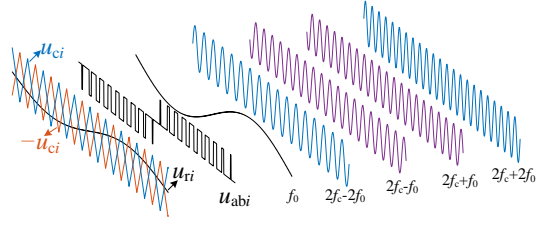

Fig. 2 PWM strategy and harmonics generation principle of the i-th H-bridge.

Based on the classical double Fourier series of u_{abi} in (3), h_{mn}^i and h_{mn} are defined as harmonic components at $[2m\omega_c+(2n-1)\omega_0]$ of u_{abi} and u_{ab}, respectively:

$$h_{mn}^i = H_{mn}^i e^{j(\omega_{mn}t+\gamma_{mn}^i)} \tag{4}$$

where the harmonic amplitude H_{mn}^i, angular frequency ω_{mn}, and phase angle γ_{mn}^i can be expressed as:

$$H_{mn}^i = \frac{2U_{dci}}{m\pi} J_{2n-1}(m\pi M_i)\cos[(m+n-1)\pi] \tag{5}$$

$$\omega_{mn} = 2m\omega_c + (2n-1)\omega_0 \tag{6}$$

$$\gamma_{mn}^i = 2m\phi_i + (2n-1)\theta_0 \tag{7}$$

According to (1), cells connected in series, h_{mn} can be expressed:

$$h_{mn} = H_{mn}e^{j(\omega_{mn}t+\gamma_{mn})} = \sum_{i=1}^{N} h_{mn}^i = e^{j(\omega_{mn}t+(2n-1)\theta_0)} \sum_{i=1}^{N} H_{mn}^i e^{j2m\phi_i} \tag{8}$$

From (2) and (8), the CHB inverter presents multiplicative switching frequency and output voltage with superior quality in ideal condition, due to the displacement angle ϕ_i in (2). That is, the harmonic distortion of the output voltage is mainly located at $2Nf_c$ (f_c=500Hz), as shown in Fig. 3. Yet, for the CHB inverter with unbalanced cells operation, such as different dc voltages or modulation indices caused by different power management among each cell, the PS-PWM technique would lose the advantage of high-quality output voltage. It is clearly shown in Fig. 3, the harmonic contents located in multiples of $2f_c$ will be presented under unbalanced conditions. As for further elaboration, the vector diagram of sideband harmonics h_{mn}^i in each cell and h_{mn} in the total output voltage has been drawn in Fig. 4, taking into account the 4-cells CHB inverter. The harmonic h_{mn} in Fig. 4 (a) can be eliminated only when the magnitudes of all individual cell harmonic components 'H_{mn}^i' are the same. Namely, the CHB inverter is operating under balanced conditions. Yet 'h_{mn}' cannot be ignored in Fig. 4 (b), when 'H_{mn}^i' are different in cells with unbalanced operating conditions [7].
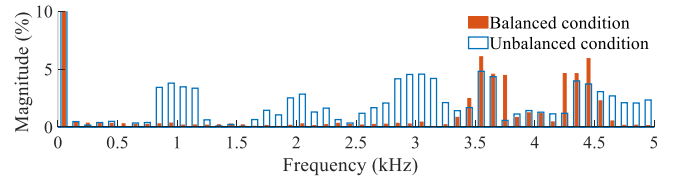

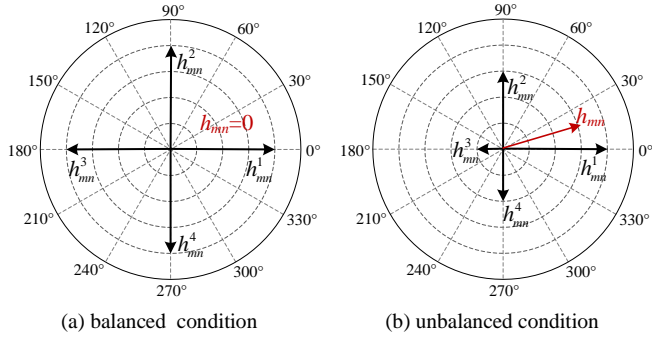Fig. 3 Harmonic spectrum of the output voltage for four cells CHB inverter.

(a) balanced condition   (b) unbalanced condition

Fig. 4 Vector diagram of the relation between harmonics in each cell.

Moreover, defining the harmonic components $h^i_{m(1-n)}$ and $h_{m(1-n)}$ as the symmetrical sideband harmonics of the selected harmonic components h^i_{mn} and h_{mn}, the harmonic component $h^i_{m(1-n)}$ can be expressed as follows, and the expression of $h_{m(1-n)}$ is similar to $h^i_{m(1-n)}$:

$$h^i_{m(1-n)} = H^i_{m(1-n)} e^{j(\omega_{m(1-n)}t + \gamma^i_{m(1-n)})}$$

$$\begin{cases} H^i_{m(1-n)} = \dfrac{2U_{dci}}{m\pi} J_{1-2n}(m\pi M_i)\cos[(m+n-1)\pi] \\ \omega_{m(1-n)} = 2m\omega_c + (1-2n)\omega_0 \\ \gamma^i_{m(1-n)} = 2m\phi_i + (1-2n)\theta_0 \end{cases} \quad (9)$$

According to the characteristic of Bessel Function, the magnitude of the sideband harmonic and its symmetrical sideband harmonic satisfy the relationship:

$$H^i_{mn} = H^i_{m(1-n)} \quad (10)$$

III. OFFLINE VARIABLE PS-PWM METHOD

To deal with the harmonic distortion induced by the unbalanced operation of the CHB inverter. The principle of the offline variable PS-PWM method investigated in [18] is as follows:

To eliminate the harmonic h_{mn} in (8), the displacement angles ϕ_i ($i=1, 2, …, N$), different from which are defined in (2), should fulfill:

$$h_{mn} = e^{j(\omega_{mn}t + (2n-1)\theta_0)} \sum_{i=1}^{N} H^i_{mn} e^{j2m\phi_i} = 0 \quad (11)$$

According to Euler's formula, (11) can be rewritten:

$$\begin{cases} \sum_{i=1}^{N} H^i_{mn} \cos(2m\phi_i) = 0 \\ \sum_{i=1}^{N} H^i_{mn} \sin(2m\phi_i) = 0 \end{cases} \quad (12)$$

Applying the new angle ϕ_i solved by (12) can achieve the complete elimination of the harmonic h_{mn}. Yet, N variables, (ϕ_i, $i=1, 2, …, N$) in expression (12) cannot be solved by two equations. To facilitate the determination of these angles, N-2 variables should be determined in advance. Besides, it is important to notice that, the equation (12) cannot always have numerical solutions due to the operational conditions of the

CHB inverter. That is, there is a limitation of the offline variable PS-PWM [18]. Taking the cascaded H-bridge inverter with 4 cells as an example, the equation system in (12) is now determined and the solution can be achieved, as 'ϕ_1' and 'ϕ_3' can be set to 0 and $\pi/2$:

$$\begin{cases} \phi_1 = 0; \\ \phi_2 = \arccos[\dfrac{-(H^1_{mn}-H^3_{mn})^2 - (H^2_{mn})^2 + (H^4_{mn})^2}{2H^2_{mn}(H^1_{mn}-H^3_{mn})}]/2; \\ \phi_3 = \pi/2; \\ \phi_4 = \arccos[\dfrac{-(H^1_{mn}-H^3_{mn})^2 + (H^2_{mn})^2 - (H^4_{mn})^2}{2H^4_{mn}(H^1_{mn}-H^3_{mn})}]/2 \end{cases} \quad (13)$$

Valid solutions for the displacement angles ϕ_2, ϕ_4 in (13) can be obtained, only when the selected sideband harmonics among each cell satisfy the constraints:

$$\begin{cases} -1 \le \dfrac{-(H^1_{mn}-H^3_{mn})^2 + (H^4_{mn})^2 - (H^2_{mn})^2}{2H^2_{mn}(H^1_{mn}-H^3_{mn})} \le 1; \\ -1 \le \dfrac{-(H^1_{mn}-H^3_{mn})^2 + (H^2_{mn})^2 - (H^4_{mn})^2}{2H^4_{mn}(H^1_{mn}-H^3_{mn})} \le 1 \end{cases} \quad (14)$$

Furthermore, similar to (11), the symmetrical sideband harmonic $h_{m(1-n)}$, relative to the harmonic 'h_{mn}', should satisfy (15) to be eliminated.

$$h_{m(1-n)} = e^{j(\omega_{m(1-n)}t + (1-2n)\theta_0)} \sum_{i=1}^{N} H^i_{m(1-n)} e^{j2m\phi_i} = 0 \quad (15)$$

Combining with (10), the equation (15) can also be rewritten as (12). The symmetrical sideband harmonic $h_{m(1-n)}$ can thereby be reduced, while the selected sideband harmonic component h_{mn} is suppressed.

However, the computational complexity of the offline variable PS-PWM method grows as the number of cells grows. The solution cannot even be obtained analytically for CHB inverters with a large number of cells, or when the harmonic magnitudes in each cell cannot satisfy the constraints. The method cannot adjust the displacement angles in real-time, with the dc-link voltage or the modulation indices changing.

IV. CLOSED-LOOP HARMONIC SUPPRESSION SCHEME

In this section, to suppress the harmonics online under all the conditions, a closed-loop harmonic suppression scheme and its implementation method are proposed.

A. Harmonic Suppression Principle

For N-cells CHB inverter, taking the harmonic h^i_{mn} in cell i as the reference, the sum of other individual cell outputs, except for cell i, is defined as $h^{ex,i}_{mn}$:

$$h^{ex,i}_{mn} = H^{ex,i}_{mn} e^{j(\omega_{mn}t + \gamma^{ex,i}_{mn})} = \sum_{j=1,j\ne i}^{N} h^j_{mn} = \sum_{j=1,j\ne i}^{N} H^j_{mn} e^{j(\omega_{mn}t + \gamma^j_{mn})} \quad (16)$$

where, $H^{ex,i}_{mn}$ and $\gamma^{ex,i}_{mn}$ represent the magnitude and phase angle of the harmonic '$h^{ex,i}_{mn}$', respectively; j represents the j-th H-bridge, except for the i-th H-bridge, ($j=1, 2, …, N, j\ne i$).

(a) $\phi_1=\pi/18$.　　　　(b) $\phi_1=\pi/9$.　　　　(c) $\phi_1=\pi/6$.　　　　(d) $\phi_1=2\pi/9$.
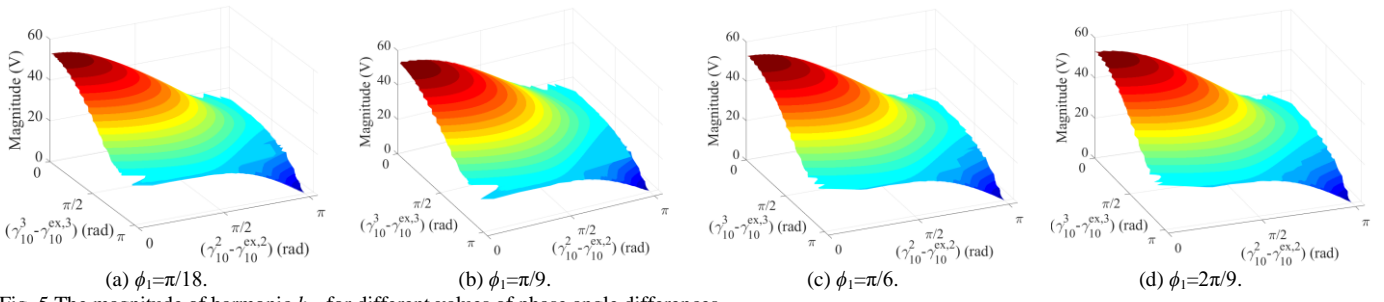
Fig. 5 The magnitude of harmonic h_{10} for different values of phase angle differences.

Therefore, h_{mn} in (8) can be rewritten:

$$h_{mn} = H_{mn}e^{j(\omega_{mn}t+\gamma_{mn})}=h_{mn}^i + h_{mn}^{\text{ex},i} \qquad (17)$$

Combining with (7), (16), and (17), the harmonic magnitude H_{mn}, and its partial derivative with respect to ϕ_i can be described as:

$$H_{mn}=\sqrt{(H_{mn}^i)^2+(H_{mn}^{\text{ex},i})^2+2H_{mn}^iH_{mn}^{\text{ex},i}\cos(\gamma_{mn}^i-\gamma_{mn}^{\text{ex},i})} \quad (18)$$

$$\frac{\partial H_{mn}}{\partial \phi_i}=\frac{-2mH_{mn}^iH_{mn}^{\text{ex},i}\sin(\gamma_{mn}^i-\gamma_{mn}^{\text{ex},i})}{\sqrt{(H_{mn}^i)^2+(H_{mn}^{\text{ex},i})^2+2H_{mn}^iH_{mn}^{\text{ex},i}\cos(\gamma_{mn}^i-\gamma_{mn}^{\text{ex},i})}} \qquad (19)$$

From (18) and (19), H_{mn} decreases monotonically as the phase angle differences $(\gamma_{mn}^i-\gamma_{mn}^{\text{ex},i}, i=1,2,\ldots,N)$ approach to π, since the value of (19) is negative at $[0, \pi]$ and positive at $(\pi, 2\pi)$. Taking harmonic magnitude H_{mn} for 3-cells CHB inverter as an example, the harmonic variation with phase differences varying is drawn in Fig. 5. It is clearly revealed from Fig. 5, the harmonic will constantly decrease with the phase angle differences approaching π in the meantime, even if the displacement angle in cell 1, ϕ_1, is different values. Fig. 6 describes the displacement angles adjustment for 3-cells CHB inverter. The phase angle in each cell is adjusted so that its phase angle difference approaches π. Combining Fig. 5 and Fig. 6, the displacement angle can be regulated in each cell separately without the effect of displacement angles in other cells. Therefore, the harmonics can be controlled to the smallest in any condition providing that the displacement angles in all the cells satisfy:

$$\gamma_{mn}^i-\gamma_{mn}^{\text{ex},i} \to \pi, \quad i=1,2,\ldots,N \qquad (20)$$

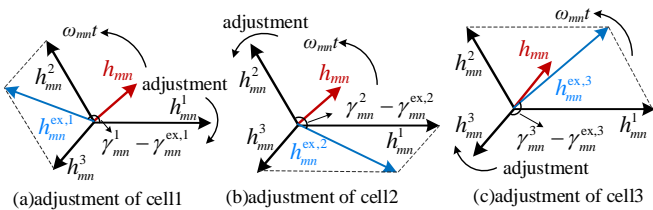(a)adjustment of cell1　　(b)adjustment of cell2　　(c)adjustment of cell3

Fig. 6 The adjustment of each cell for 3-cells CHB inverter.

Fig. 8 (a) describes the flow chart to suppress the selected harmonics, and four parts mainly include: 1) Obtaining the voltages of the CHB inverter and the i-th H-bridge: u_{ab}, $u_{\text{ab}i}$; 2) Extracting harmonics selected for suppression: h_{mn} and h_{mn}^i; 3) Obtaining the angle difference $(\gamma_{mn}^i-\gamma_{mn}^{\text{ex},i})$ in each cell; 4)

Obtaining the displacement angle compensation $\Delta\phi_i$ in each cell based on (20), and adjusting the displacement angle of the carrier to ϕ'_i in real-time. It should be highlighted that, the pivotal steps are the angle difference $(\gamma_{mn}^i-\gamma_{mn}^{\text{ex},i})$ extraction and the displacement angles adjustment.

B. The implement of the closed-loop harmonic suppression scheme.

To carry out the closed-loop harmonic suppression scheme, the implemented method based on the "dq frame" is proposed.

As shown in Fig. 7, taking the phase angle of harmonic h_{mn}^i in cell i as the reference, the harmonic component h_{mn}^k in the cell k can be expressed in the "dq frame", of which the angular velocity is equal to ω_{mn}:

$$(h_{mn}^{k\text{dq}})_i=h_{mn}^k e^{-j(\omega_{mn}t+\gamma_{mn}^i)} = H_{mn}^k e^{j(\gamma_{mn}^k-\gamma_{mn}^i)} \qquad (21)$$

$$\begin{cases} (h_{mn}^{k\text{d}})_i=H_{mn}^k\cos(\gamma_{mn}^k-\gamma_{mn}^i) \\ (h_{mn}^{k\text{q}})_i=H_{mn}^k\sin(\gamma_{mn}^k-\gamma_{mn}^i) \end{cases}, \quad (k,i\in 1,2,\ldots,N) \qquad (22)$$

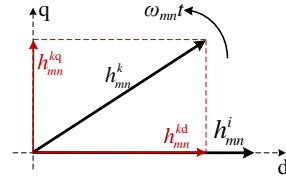

Fig. 7 Harmonic components in the dq frame.

Combining (17) and (22), the harmonic h_{mn} in the total output voltage of the N-cells CHB inverter can be expressed in "dq frame" as follows:

$$\begin{cases} (h_{mn}^{\text{d}})_i=(h_{mn}^{i\text{d}})_i+(h_{mn}^{\text{ex},i\text{d}})_i=H_{mn}^i+H_{mn}^{\text{ex},i}\cos(\gamma_{mn}^{\text{ex},i}-\gamma_{mn}^i) \\ (h_{mn}^{\text{q}})_i=(h_{mn}^{i\text{q}})_i+(h_{mn}^{\text{ex},i\text{q}})_i=H_{mn}^{\text{ex},i}\sin(\gamma_{mn}^{\text{ex},i}-\gamma_{mn}^i) \end{cases} \qquad (23)$$

$$(i\in 1,2,\ldots,N)$$

Substituting (20) into (23), the components in the "dq frame" meet:

$$\begin{cases} (h_{mn}^{\text{d}})_i=(h_{mn}^{i\text{d}})_i+(h_{mn}^{\text{ex},i\text{d}})_i=H_{mn}^i+H_{mn}^{\text{ex},i}\cos(\gamma_{mn}^i-\gamma_{mn}^{\text{ex},i}) \to H_{mn}^i-H_{mn}^{\text{ex},i} \\ (h_{mn}^{\text{q}})_i=(h_{mn}^{i\text{q}})_i+(h_{mn}^{\text{ex},i\text{q}})_i=-H_{mn}^{\text{ex},i}\sin(\gamma_{mn}^i-\gamma_{mn}^{\text{ex},i}) \to 0 \end{cases} \qquad (24)$$

It can be noticed from (24), the suppression for the harmonic component h_{mn}, in unbalanced operating conditions of different cells, depends on the harmonic component in the q-axis, $(h_{mn}^{\text{q}})_i$, approaching to π:
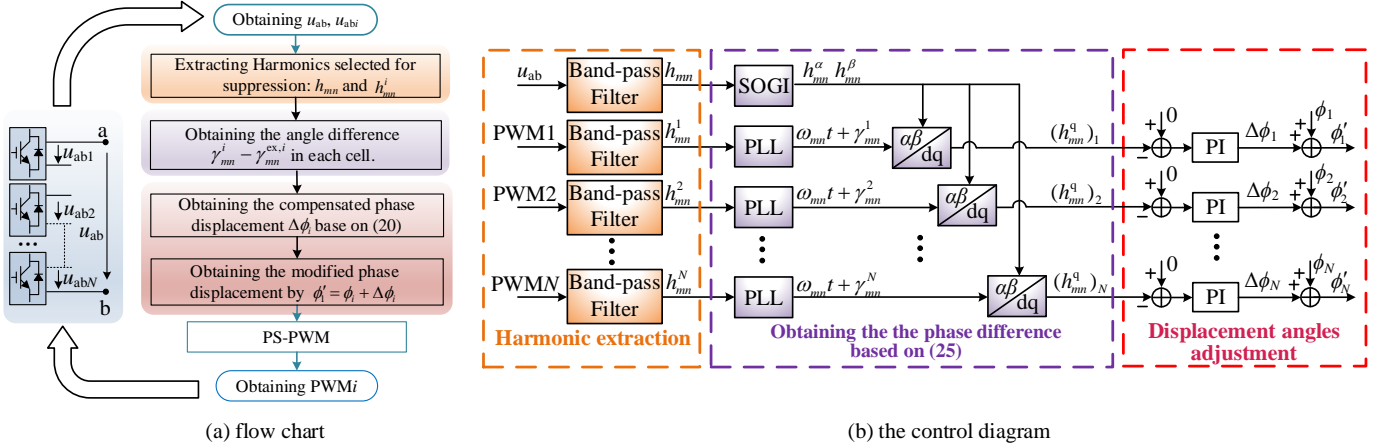
(a) flow chart   (b) the control diagram

Fig. 8 The control diagram of the proposed closed-loop harmonic suppression scheme.

$$(h_{mn}^{q})_i \to 0, \quad i = 1, 2, 3, ..., N \qquad (25)$$

As can be observed from previous analysis, the control diagram of the proposed closed-loop harmonic suppression scheme described in Fig. 8 (b), the detailed steps to adjust the displacement angles are as follows: 1) Obtaining the output voltages of the CHB inverter and the ith H-bridge: u_{ab} and u_{abi}, by sampling directly from the ac side of CHB inverter, or be synthesized by dc voltage of each cell and output pulse state of the controller, or other methods. 2) Harmonics selected for suppression, h_{mn} and h_{mn}^{i}, are extracted by the band-pass filter. 3) As the key step to be considered, the second-order generalized integrator (SOGI) and the phase-locked loop (PLL) are adopted to obtain the harmonic component in q axis, h_{mn}^{q}. 4) It is also important to notice that, the displacement angle compensation $\Delta\phi_i$ is obtained by the PI controller based on (25), and adjusting the displacement angle of the carrier to ϕ'_i in real-time.

V. SIMULATION AND EXPERIMENTAL RESULTS

The simulation and the scaled-down experimental test of four-cells CHB are executed to validate the proposed online closed-loop harmonic suppression scheme. The CHB laboratory prototype shown in Fig. 9 has been used to carry out the experiments. Each power cell is supplied by an isolated dc source. The CHB inverter is managed by the microcontroller TMS320F28335 digital signal processor from Texas Instruments. The system parameters are shown in TABLE I. The results applying the conventional PS-PWM, offline variable PS-PWM (off. var. PS-PWM), and the proposed closed-loop harmonic suppression method are compared. All considered cases, chosen randomly considering different dc voltages and modulation indices, are listed in TABLE II. The sideband harmonics at $2f_c$, $4f_c$, and $6f_c$, (950Hz, 2150Hz, and 2850Hz), are suppressed to verify the effectiveness of the proposed method.
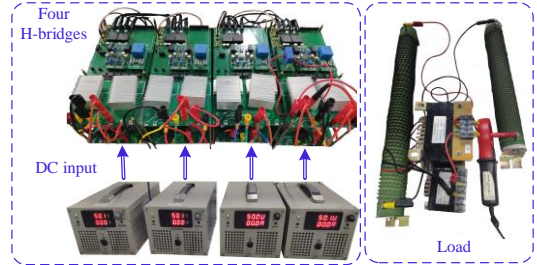

Fig. 9 The experiment platform.

TABLE I
SYSTEM PARAMETERS

Parameters	Value
Sampling time $t_s/\mu s$	100
Switching frequency f_c/Hz	500
The inductance of ac side L_s/mH	15
The resistance load of ac side R_s/Ω	20
The dc-link capacitor C/mF	3.3

TABLE II
SCENARIOS OF UNBALANCED CONDITION

Case	DC voltages U_{dci}/V	Modulation indices M_i/p.u.
I	[50 50 50 50]	[0.7 0.75 0.6 0.8]
II	[50 60 55 70]	[0.8 0.8 0.8 0.8]
III	[70 50 55 60]	[0.8 0.95 0.8 0.7]

The three cases in TABLE II are carried out in consecutive 15 ms intervals. Observing the magnitudes of harmonics at 950 Hz, 2150 Hz, and 2850 Hz in Fig. 10 (a), (c), and (e), harmonics can be suppressed effectively by the proposed method for all the cases. Yet, the offline variable PS-PWM can only achieve the suppression of harmonics at 950 Hz in Case I and 2850 Hz in Case III, since there are no numerical solutions of the displacement angles for other operational conditions. Additionally, as shown in Fig. 10 (b), (d), and (f), it has to be highlighted that the harmonics at 1050 Hz, 1850 Hz, and 3150 Hz, which are symmetrical sideband harmonics with 950 Hz, 2150 Hz, and 2850 Hz, also have a good suppression performance. Taking into account the fact in Fig. 10, the proposed method can suppress harmonics in real-time, with the operational conditions changing. And the proposed method permits obtaining a superior harmonic performance in a wider range of the CHB operational conditions.
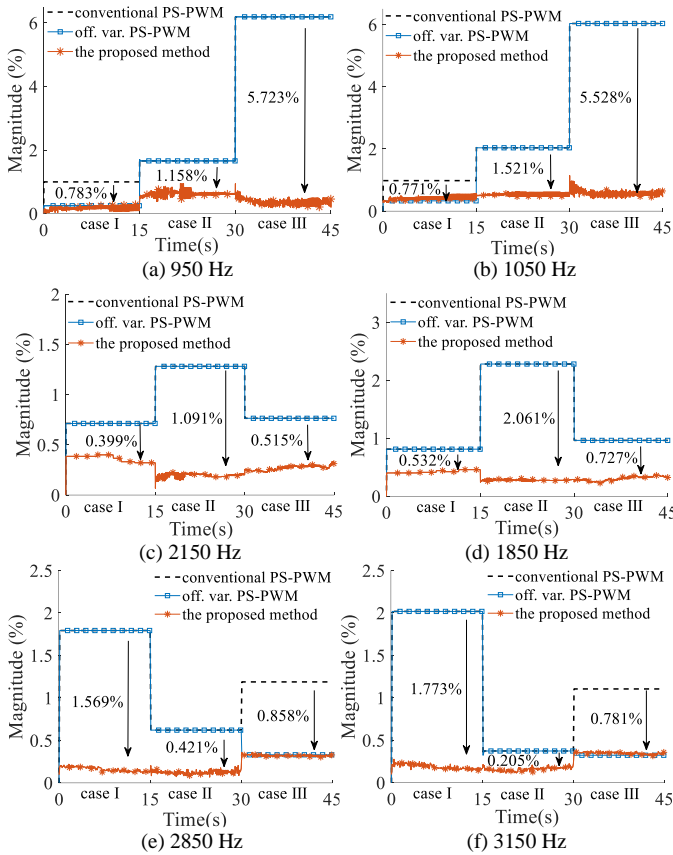
Fig. 10 Harmonics at 950 Hz, 2150 Hz, or 2850 Hz are suppressed. (1050 Hz, 1850 Hz, and 3150 Hz are symmetrical sideband harmonics with 950 Hz, 2150 Hz, and 2850 Hz, respectively)

Fig. 11 describes the displacement angles in real-time. For all the cases, it can be seen that the displacement angles are adjusted in real-time and become stable by the proposed method, when the dc-link voltage or the modulation indices are changing. Yet, only when the harmonics at 950 Hz and 2850 Hz to be suppressed for Case I and Case III, respectively, new displacement angles can be solved by the offline variable PS-PWM, due to the constraints in (14). Therefore, the proposed closed-loop harmonic suppression method presents a superior harmonic performance in a wider range of the CHB operational conditions.

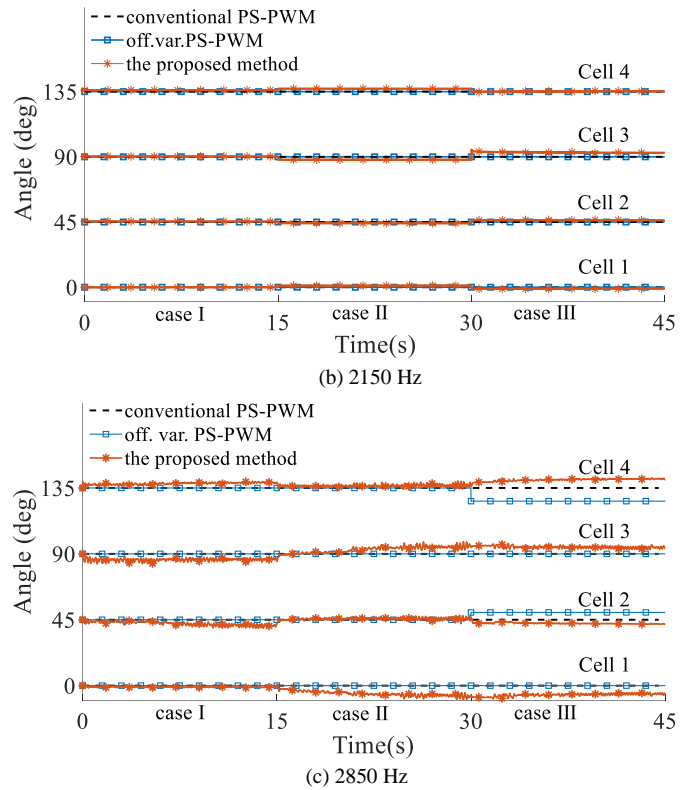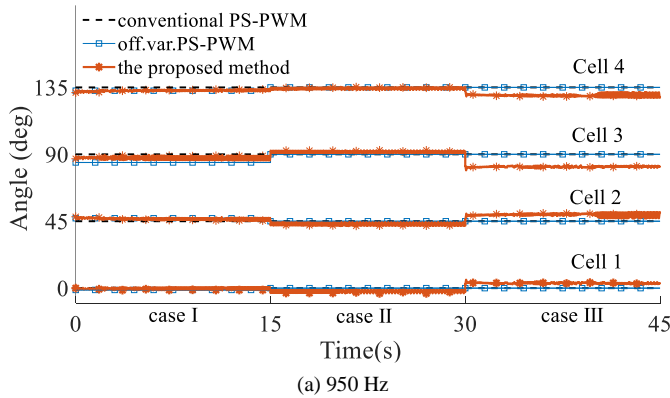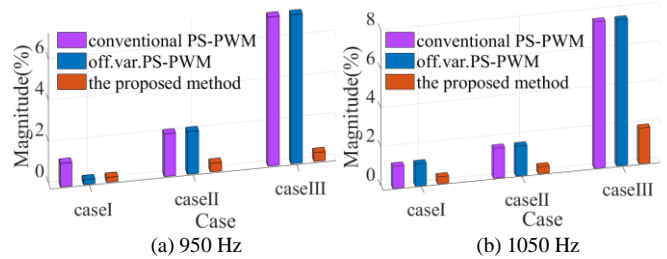
(a) 950 Hz

(b) 2150 Hz

(c) 2850 Hz

Fig. 11 The displacement angles when harmonics at 950 Hz, 2150 Hz, or 2850 Hz are suppressed.

Fig. 12 shows the harmonic magnitudes of experimental results for the three cases in TABLE II. Based on the harmonic magnitudes at 950 Hz, 2150 Hz, and 2850 Hz described in Fig. 12 (a), (c), and (e), the proposed method in this article is visibly effective to suppress the selected harmonic. According to Fig. 12 (b), (d), and (f), the symmetrical sideband harmonics (1050 Hz, 1850 Hz, 3150 Hz) also have a good suppression performance. Yet, for the offline variable PS-PWM technique, which calculates the phase angles offline, only the harmonic at 950 Hz in Case I and 2850 Hz in Case III, where numerical solutions of the phase angles exist, can be minimized. It is not suitable for other cases in TABLE II.

Therefore, the proposed method in this article is effective for any conditions to suppress the selected harmonic in real-time. And it is also effective under varied operational conditions, or the harmonic frequency selected for suppression changes with the requirements of practical application scenario.
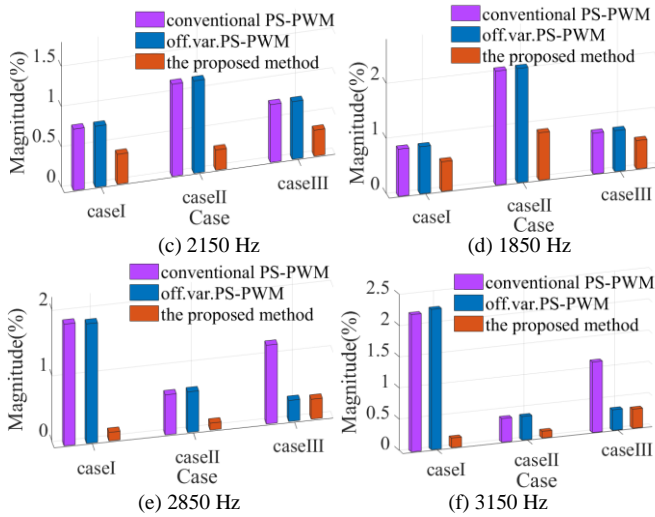

(a) 950 Hz

(b) 1050 Hz

Fig. 12 The harmonic magnitudes when harmonics at 950 Hz, 2150 Hz, or 2850 Hz are controlled to be suppressed. (1050 Hz, 1850 Hz, and 3150 Hz are symmetrical sideband harmonics with 950 Hz, 2150 Hz, and 2850 Hz, respectively)

Furthermore, as expected, the proposed method has no adverse effect on ac current control. For instance, the harmonic ratio of the ac current (HRI) at 950 Hz and the total harmonic distortion (THD) of the output voltage can also be reduced to some extent by the proposed method shown in Fig. 13.
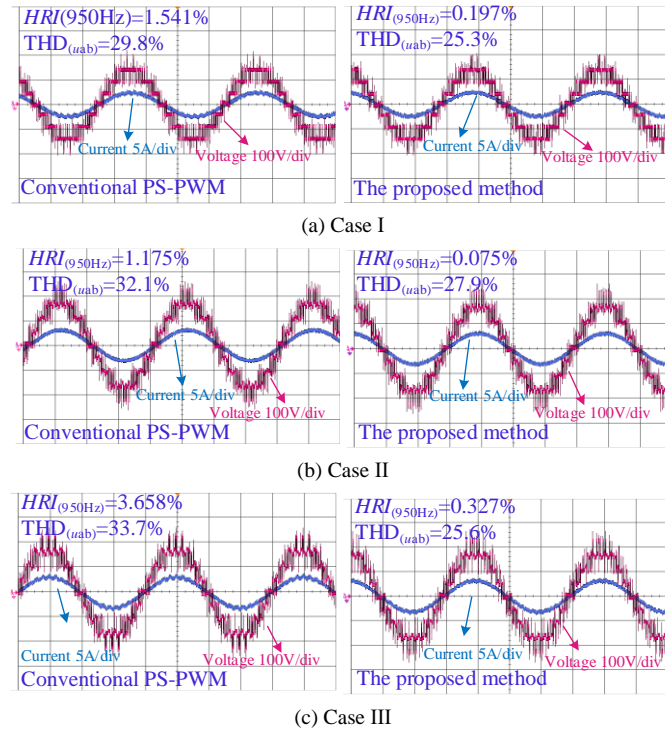

Fig. 13 The ac voltages and currents based on the proposed method to suppress harmonics at 950 Hz.

VI. CONCLUSIONS

The closed-loop harmonic suppression scheme is proposed in this article for CHB converter, and according to the analysis, the main conclusions can be drawn as follows:

1) The proposed harmonic suppression scheme can regulate the displacement angles of the triangular carriers in different cells online, and suppress specific harmonics in real-time. The symmetrical sideband harmonics with the selected sideband harmonics also have a good suppression performance.

2) In the proposed method, the displacement angle regulation is much simpler than the offline variable PS-PWM. The complicated numerical solution of the phase angles is effectively avoided.

3) The proposed method is effective to suppress harmonics in real-time, when the operating conditions change, or the harmonic frequency selected for suppression changes with the requirements of practical application scenario.

4) The proposed method for CHB inverters can effectively operate without the limitation of cell numbers.

REFERENCES

[1] N. B. Y. Gorla, S. Kolluri, M. Chai, and S. K. Panda, "A Comprehensive Harmonic Analysis and Control Strategy for Improved Input Power Quality in a Cascaded Modular Solid-State Transformer," *IEEE Trans. Power Electron*, vol. 34, no. 7, pp. 6219-6232, July 2019.

[2] Z. Yang, J. Sun, Y. Tang, M. Huang, and X. Zha, "An integrated dual voltage loop control for capacitance reduction in CHB-based regenerative motor drive systems," *IEEE Trans. Ind. Electron.*, vol. 66, no. 5, pp. 3369–3379, May 2019.

[3] Z. Yang, J. Sun, X. Zha, and Y. Tang, "Power decoupling control for capacitance reduction in cascaded-H-bridge-inverter-based regenerative motor drive systems," *IEEE Trans. Power Electron.*, vol. 34, no. 1, pp. 538–549, Jan. 2019.

[4] G. P. Adam, I. A. Abdelsalam, K. H. Ahmed, and B. W. Williams, "Hybrid multilevel inverter with cascaded H-bridge cells for HVDC Applications: Operating principle and scalability," *IEEE Trans. Power Electron*, vol. 30, no. 1, pp. 65–77, Jan. 2015.

[5] Q. Zhang and K. Sun, "A flexible power control for PV-battery-hybrid system using cascaded h-bridge inverters," *IEEE J. Emerg. Sel. Topics Power Electron.*, vol. 7, no. 4, pp. 2184–2195, Dec. 2019.

[6] Y. Lu, Z. Liu, J. Kong, D. Tang, J. Yu, J. Ji, "A Fundamental Voltage and Harmonics Elimination Control Strategy for Single-phase Cascaded Off-grid Photovoltaic-storage system Using Hybrid Modulation," in *Energy Conversion Congress and Exposition (ECCE) 2020 IEEE*, pp. 321-327, 2020.

[7] V. G. Monopoli, Y. Ko, G. Buticchi and M. Liserre, "Performance Comparison of Variable-Angle Phase-Shifting Carrier PWM Techniques," *IEEE Trans. Ind. Electron.*, vol. 65, no. 7, pp. 5272-5281, July 2018.

[8] Hanson D J. "A transmission SVC for National Grid Company plc incorporating a ±75 MVAr STATCOM," *Flexible Ac Transmission Systems-the Facts. IET*, 1998:5/1-5/8.

[9] Scarfone A W, Oberlin B K, Luca J P J D, et al. "A ±150 MVAr STATCOM for Northeast Utilities' Glenbrook substation," *Power Engineering Society General Meeting. IEEE*, 2003.

[10] Y. Yu, G. Konstantinou, B. Hredzak, and V. G. Agelidis, "Operation of Cascaded H-Bridge Multilevel Converters for Large-Scale Photovoltaic Power Plants Under Bridge Failures," *IEEE Trans. Ind. Electron.*, vol. 62, no. 11, pp. 7228-7236, Nov. 2015.

[11] M. Malinowski, K. Gopakumar, J. Rodriguez and M. A. Pérez, "A Survey on Cascaded Multilevel Inverters," *IEEE Trans. Ind. Electron.*, vol. 57, no. 7, pp. 2197-2206, July 2010.

[12] Q. Zhang and K. Sun, "A flexible power control for PV-battery-hybrid system using cascaded h-bridge converters," *IEEE J. Emerg. Sel. Topics Power Electron.*, vol. 7, no. 4, pp. 2184–2195, Dec. 2019.

[13] L. Liu, H. Li, Z. Wu, and Y. Zhou, "A Cascaded Photovoltaic System Integrating Segmented Energy Storages With Self-Regulating Power Allocation Control and Wide Range Reactive Power Compensation," *IEEE Trans. Power Electron.*, vol. 26, no. 12, pp. 3545-3559, Dec. 2011.

[14] S. Wang, N. Jiao, J. Ma, T. Liu and X. Liu, "Analysis and Optimization of Voltage Balancing Control Limits for Cascaded H-Bridge Rectifiers," *IEEE Trans. Ind. Electron.*, doi: 10.1109/TIE.2020.3032874.

[15] M. Liserre, V. G. Monopoli, A. Dell'Aquila, A. Pigazo, and V. Moreno, "Multilevel phase-shifting carrier PWM technique in case of non-equal dc-link voltages," in *Proc. 32nd Annu. Conf. IEEE Ind. Electron.*, 2006, pp. 1639–1642.

[16] Y. Sun, J. Zhao and Z. Ji, "An improved CPS-PWM method for cascaded multilevel STATCOM under unequal losses," in *IECON 2013 - 39th Annual Conference of the IEEE Industrial Electronics Society, Vienna*, 2013, pp. 418-423.

[17] M. Schuck, A. D. Ho, and R. C. Pilawa-Podgurski, "Asymmetric interleaving in low-voltage CMOS power management with multiple supply rails," *IEEE Trans. Power Electron.*, vol. 32, no. 1, pp. 715–722, Jan. 2017.

[18] A. Marquez et al., "Variable-angle phase-shifted PWM for multilevel three-cell cascaded H-bridge inverters," *IEEE Trans. Ind. Electron.*, vol. 64, no. 5, pp. 3619–3628, May 2017.

[19] A. Marquez, J. I. Leon, V. G. Monopoli, S. Vazquez, M. Liserre, and L. G. Franquelo, "Generalized Harmonic Control for CHB Inverters With Unbalanced Cells Operation," *IEEE Trans. Ind. Electron.*, vol. 67, no. 11, pp. 9039-9047, Nov. 2020.

[20] V. G. Monopoli, A. Marquez, J. I. Leon, Y. Ko, G. Buticchi, and M. Liserre, "Improved harmonic performance of cascaded H-bridge inverters with thermal control," *IEEE Trans. Ind. Electron.*, vol. 66, no. 7, pp. 4982–4991, Jul. 2019.

[21] A. Marquez et al., "Sampling-Time Harmonic Control for Cascaded H-Bridge Inverters With Thermal Control," *IEEE Trans. Ind. Electron.*, vol. 67, no. 4, pp. 2776-2785, Apr. 2020.

[22] F. Eroglu, A. O. Arslan, M. Kurtoglu, and A. M. Vural, "Generalized adaptive phase-shifted PWM for single-phase seven-level cascaded H-bridge multilevel inverters," in *2018 5th International Conference on Electrical and Electronic Engineering (ICEEE)*, Istanbul, 2018, pp. 7-12.

[23] X. Zha, Z. Yang, J. Gong, S. Li, F. Liu, and M. Huang, "Asymmetrical carrier phase-shifted pulse-width modulation for partly regenerative inverter," *IET Power Electron.*, vol. 10, no. 4, pp. 442–450, Mar. 2017.

[24] M. Schuck and R. C. N. Pilawa-Podgurski, "Ripple minimization through harmonic elimination in asymmetric interleaved multiphase DC-DC inverters," *IEEE Trans. Power Electron.*, vol. 30, no. 12, pp. 7202–7214, Dec. 2015.

[25] S. Li, Z. Yang, Q. Li, J. Gong, J. Sun, and X. Zha, "Asymmetrical phase-shifting carrier pulse-width modulation for harmonics suppression in cascaded multilevel inverter under unbalanced dc-link voltages," in *Proc. IEEE Energy Convers. Congr. Expo.*, Sep. 2015, pp. 6804–6810.

[26] M. Schuck and R. C. N. Pilawa-Podgurski, "Ripple minimization through harmonic elimination in asymmetric interleaved multiphase DC-DC inverters," *IEEE Trans. Power Electron.*, vol. 30, no. 12, pp. 7202–7214, Dec. 2015.

[27] A. Marquez, "High-quality output voltage of multilevel cascaded h-bridge inverters with large number of cells with unequal DC voltages," in *Proc. IEEE 13th Int. Conf. Compat. Power Electron. Power Eng.*, Apr. 2019.

[28] X. J. Cai, Z. X. Wu, Q. F. Li, and S. X. Wang, "Phase-shifted carrier pulse width modulation based on particle swarm optimization for cascaded H-bridge multilevel inverters with unequal dc voltages," *Energies*, 2015.

[29] F. Eroğlu, M. Kurtoğlu, A. O. Arslan, and A. M. Vural, "Harmonic reduction under unbalanced operating conditions of PV-connected cascaded H-bridge multilevel inverters using fault tolerant adaptive phase-shifted pulse width modulation," *Int. Trans. Electr. Energy Syst.*, vol. 29, no. 4, p. e2814, Apr. 2019.

[30] D. Holmes and T. Lipo, Pulse Width Modulation for Power Inverters: Principles and Practice. Hoboken, NJ, USA: Wiley, 2003.